Available online at www.sciencedirect.com

ScienceDirect

Ceramics International 42 (2016) 1352–1360

CERAMICS INTERNATIONAL

www.elsevier.com/locate/ceramint

$CaTiO_3$ and $Ca_{1-3x}Sm_xTiO_3$: Photoluminescence and morphology as a result of Hydrothermal Microwave Methodology

Ivo M. Pinatti[a], Tatiana M. Mazzo[b], Rosana F. Gonçalves[c], José A. Varela[d], Elson Longo[d], Ieda L.V. Rosa[a,*]

[a]INCTMN, LIEC, Chemistry Department, Federal University of São Carlos, P.O. Box 676, 13565-905 São Carlos, SP, Brazil
[b]Instituto de Ciência e Engenharia do Mar-Federal University of São Paulo-UNIFESP/Campus Baixada Santista, Av. Alm. Saldanha da Gama, 89 – Ponta da Praia, Santos, SP CEP: 11030-400, Brazil
[c]UNIFESP, Federal University of São Paulo, Rua Prof. Artur Riedel, 275, SP, 09972-270 Diadema, SP, Brazil
[d]INCTMN, LIEC, Chemistry Institute, State University of São Paulo, UNESP, P.O. Box 355, 14800-900 Araraquara, SP, Brazil

Received 20 May 2015; received in revised form 13 August 2015; accepted 14 September 2015
Available online 24 September 2015

Abstract

Calcium titanate ($CaTiO_3$ – CT) and samarium doped calcium titanate ($CaTiO_3$:Sm^{3+} – CT:Sm) powders in different Sm^{3+} concentrations (0.5–5.0% molar ratio of Sm^{3+}) were obtained by the Hydrothermal Microwave Methodology at 140 °C for 16 min. These crystals were structurally characterized by X-ray diffraction (XRD) and micro-Raman (MR) spectroscopy. Field emission scanning electron microscopy images were employed to observe the shape and size of the crystals. The optical properties were investigated by ultraviolet–visible (UV–Vis) absorption and photoluminescence (PL) measurements. The XRD indicated structural organization at long range while MR revealed short range order for all undoped and Sm-doped samples. Morphological analysis revealed a new cubic morphology for CT:Sm, presenting an average size of 3.0 μm. Further, the ultraviolet–visible absorption spectra indicated the existence of intermediary energy levels within the band gap. The maximum intensity PL emission occurred due to $^4G_{5/2} \rightarrow {}^6H_{7/2}$ and $^4G_{5/2} \rightarrow {}^6H_{9/2}$ transitions of Sm^{3+}. CIE chromaticity coordinates of the samples were determined and support these materials are promising candidates for applications as phosphors in the visible orange range. This research concluded that the methodology employed here was responsible for the presence of unusual and interesting properties for these new luminescent materials.

Keywords: Hydrothermal Microwave; Calcium titanate; Samarium; Photoluminescence

1. Introduction

In recent years, materials with new morphologies have attracted great attention due to their applications in many fields [1–3]. Calcium titanate (CT) is a perovskite-type ceramic with outstanding properties that can be used as biomaterials for defect healing and bone regeneration *in vivo* [4], dielectric resonators in wireless communication systems [5] and high photocatalytic activity of decomposing water [6] in H_2 and O_2. Despite these applications, most attention has been devoted to the photoluminescence (PL) properties of ceramic materials because of the development of advanced displays for multimedia applications. The field emission display (FED) is one of the best candidates for advanced flatpanel applications [7] and the CT doped rare earth materials has significant PL properties at room temperature for this purpose [8].

The spectroscopic properties of rare earth materials have been studied on the basis of the crystal field splitting of the $^{2S+1}L_J$ manifolds of the $4f^5$ configuration of the Sm^{3+} ion. The rare-earth ions have a partially filled 4f shell that is shielded by $5s^2$ and $5p^6$ orbitals and the emission transitions result in sharp lines in the optical spectra. The luminescence of Sm^{3+} is situated in the orange spectral region and results from

*Corresponding author. Tel./fax: +55 16 3351 9308.
E-mail address: ilvrosa@ufcar.br (I.L.V. Rosa).

http://dx.doi.org/10.1016/j.ceramint.2015.09.074
0272-8842/

the intraconfigurational f–f transitions from the $^4G_{5/2}$ level to the ground state $^6H_{5/2}$ one, as well as to higher [9] levels ^6H_J ($J > 5/2$). Since Sm^{3+} has an odd electron configuration it is considered a Kramer's ion, which requires that the electronic states must be at least doubly degenerate by the ligand-field for any chemical environment, and the maximum number of Stark components for a $^{2S+1}L_J$ state is $J+1/2$ for any symmetry lower than cubic [10]. The applications of this ions involves their use in *WLEDs* [11], visible lasers [12], enhance ionic conductivity [13], hybrid materials [14], rare earth codoping [15], study of magnetic properties [16] and can also be used as a probe in multi-analytical assays [17]. Sm^{3+} shows different quenching channels through the $^4G_{5/2}$ emitting level, and because of the energy gap between this level and the underlying $^6F_{11/2}$, it is possible to have long lifetime in low doping concentration and the multiphonon non-radiative decay is also rarely observed [12].

Besides CT powders have been reported in different methodologies (mecanochemical [18], conventional hydrothermal [19], coprecipitation [20]), the literature register on the synthesis of CT:Sm powders only divulged their preparation by the solid-state reaction [21] and polymeric precursor method [22–24]. For the first time, these materials were synthesized by a cutting-edge technology called as Hydrothermal Microwave Methodology (HTMW). The materials obtained by this approach showed different morphology and photoluminescence properties when compared the literature data. This methodology has the advantage of using low temperature and short annealing times, which can be entitled as an environmental friendly procedure. Sm^{3+} concentrations were varied in the CT matrix in order to evaluate the maximum photoluminescence intensity and the quenching concentration of this ion, as well as their influence in the structural and morphological behavior.

2. Experimental section

CT and $Ca_{1-3x}Sm_xTiO_3$ (x=0.5%, 1.0%, 3.0% and 5.0% mol ratio of Sm^{3+} ions) powders were synthesized using $[Ti(OC_3H_7)_4]$ (99,99%, Aldrich), $CaCl_2 \cdot 2H_2O$ (99.9%, Merck), Sm_2O_3 (99.999%, Aldrich) and KOH (99%, Merck). The solutions were prepared as following. Firstly, 0.01 mol of the $[Ti(OC_3H_7)_4]$ was slowly added in 25 mL of deionized water close to the temperature of 0 °C under magnetic stirring (Reaction 1). In a similar way, 0.01 mol of the $CaCl_2 \cdot 2H_2O$ was dissolved in 25 mL of deionized water in room temperature, giving rise to a transparent solution. For CT:Sm samples were stoichiometrically added 0.5%, 1.0%, 3.0% and 5.0% mol of the $SmCl_3$ solution in the Ca^{2+} solution resulting in CT0.5, CT1, CT3 and CT5 respectively. The Sm solution was prepared thought the dissolution of Sm_2O_3 in some drops of concentrated HCl and water until a yellow transparent solution was obtained. The two precursor solutions (Titanium and Calcium/Sm) were then mixed under constant magnetic stirring, with 50 mL of a 6.0 M KOH solution, which act as a mineralizer. This procedure promotes the coprecipitation of the amorphous titanium oxide ($TiO(OH)_2$), as well as calcium ($Ca(OH)_2$) and samarium ($Sm(OH)_3$) hydroxides to form the reactional mixture (Reactions 2–4). This mixture was then transferred to a 110 mL Teflon® autoclave reaching 90% of its total volume allowing the maximum pressure efficiency. The autoclave was finally sealed and placed in the HTMW system using 2.45 GHz microwave radiation with maximum power of 800 W. The reactional mixture was heated at 140 °C under nominal heating rate of 140 °C/min (at 800 W) by direct interaction of water molecules with microwaves radiation and remained under constant pressure of 2.5 Bar for 16 min (Reactions 5 and 6). For comparison, a solution without exposure to microwave radiation was prepared in the same way. After that, the autoclave was naturally cooled to room temperature. Thus, the solid product was water washed for several times until neutral pH, and then, dried at 80 °C for 12 h.

$$Ti[OCH(CH_3)_2]_{4(l)} + 2H_2O_{(l)} \rightarrow TiO_{2(s)} + 4(CH_3)_2CHOH_{(l)} \quad (1)$$

$$Ca^{2+}_{(aq)} + 2OH^-_{(aq)} \rightarrow Ca(OH)_{2(s)} \quad (2)$$

$$TiO_{2(s)} + 4OH^-_{(aq)} \rightarrow TiO(OH)_{2(s)} + H_2O_{(l)} \quad (3)$$

$$Sm^{3+}_{(aq)} + 3OH^-_{(aq)} \rightarrow Sm(OH)_{3(s)} \quad (4)$$

$$TiO(OH)_{2(s)} + Ca(OH)_{2(s)} \xrightarrow{\text{microwave}} CaTiO_{3(s)} + 2H_2O_{(l)} \quad (5)$$

$$x\,Ca(OH)_{2(s)} + x\,Sm(OH)_{3(s)} + TiO(OH)_{2(s)} \xrightarrow{\text{microwave}} Ca_{1-3x}Sm_xTiO_{3(s)} + y\,H_2O_{(l)} \quad (6)$$

2.1. Measurements and characterization

CT and CT:Sm powders were characterized by XRD in a Rigaku Dmax 2500PC diffractometer, using a Cu Kα (λ=1.5406 Å) radiation in order to determine the structural evaluation. The data were collected from 20° to 75° in 2θ range with 0.5° divergence slit and 0.3 mm receiving slit, using fixed-time mode, scan speed 2°/min with 0.02° step size and 1 s/point. The micro-Raman scattering (MRS) measurements were performed using a 514.5 nm line of an argon ion laser as excitation source. The power was kept at 9 mW and a 100 mm lens was used. The spectra were recorded using a T-64000 (Jobin-Yvon) triple monochromator coupled to a CCD detector. UV–vis absorption spectra of these samples were taken using total diffuse reflectance mode in a Cary 5 G equipment. The Photoluminescence (PL) data of the CT:Sm powders were obtained in a Jobin Yvon – Fluorolog III spectrofluorometer under excitation of a 450 W Xenon lamp. Luminescence lifetime measurements were carried out as well using a 1940D model spectrophosphorometer coupled to the spectrofluorometer. The chromaticity coordinates were calculated with SpectraLux® software. Finally, microstructural characterization was performed by field emission gun scanning electron microscopy (FE-SEM) using a Zeiss Supra™ 35 equipment. All these measurements were performed at room temperature.

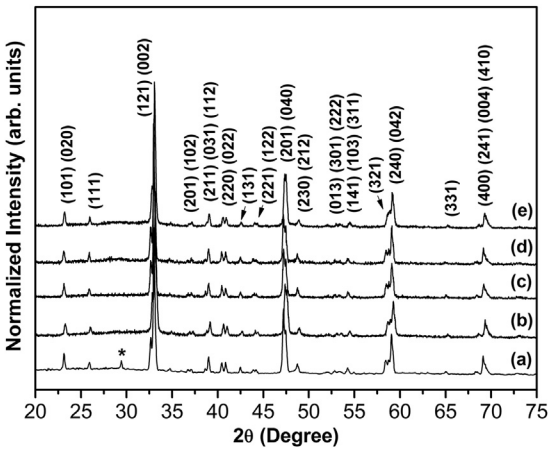

Fig. 1. XRD patterns of CT and CT:Sm powders synthesized at 140 °C for 16 min. (a) CT, (b) CT0.5, (c) CT1, (d) CT3 and (e) CT5. The "*" stands for $CaCO_3$ phase.

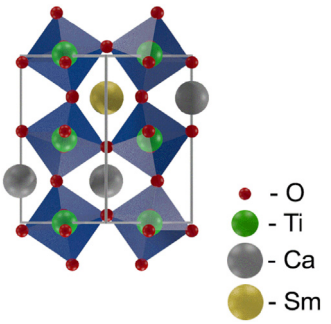

Fig. 2. Simulated orthorhombic lattice of the CT:Sm samples annealed at 140 °C for 16 min.

3. Results and discussion

3.1. X ray diffraction (XRD)

The structural order at log-range of the crystals was evaluated by XRD patterns analysis. Fig. 1 shows the diffraction patterns of CT and CT:Sm powders synthesized at 140 °C for 16 min using the HTMW method. The diffraction patterns are in accordance with JCPDS card (No. 22-0153) of the perovskite-type $CaTiO_3$ crystal. One small peak in $2\theta = 30^\circ$ resulted by the impurities of $CaCO_3$ (JCPDS No. 5-543) was observed just in the sample CT, which is associated to an incomplete reaction. We can also assume the phase as orthorhombic with *Pbnm* space group and there was no change in the overall crystal structure as Sm^{3+} concentration increased up to 5.0 mol%. The comparison solution did not show phase characteristic to CT, then it was not presented here.

Paris et al. [25] studied the Sm^{3+} doping titanates and the results obtained showed that the phase transition is dependent upon the samarium content. Once phase transition or structural distortion was not observed, long-range order were obtained for all Sm additions used here.

In literature it is possible to find different papers indicating that lanthanide substitution usually occurs in both A and B site of perovskites [26,27], but A position is favorable when considering electronic density and coordination number of the ions involved [28,29]. This statement indicates the substitution of Ca^{2+} by the Sm^{3+} in the A site ($ATiO_3$) of the CT samples, which also supports the doping calculation, that was done subtracting Ca^{2+} in order to insert the concentrations of Sm^{3+}. These results confirm the crystallinity of all samples and those doping amounts did not provoke changes in the material analyzed.

In Fig. 2 is represented the simulated orthorhombic lattice of the CT:Sm samples annealed at 140 °C for 16 min by the HTMW method. This unit cell was modeled through the Visualization for Electronic and Structural Analysis (VESTA) program, version 3 for Windows [30]. The image illustrates the substitution of Sm^{3+} in the cubo-octahedral sites (CaO_{12}) of Ca^{2+} while Ti^{4+} remains unchanged in the octahedral sites (TiO_6).

3.2. Micro-Raman scattering (MRS)

Micro-Raman spectroscopy is a powerful tool in analyzing configuration of ceramic materials. Throughout this technique is possible to observe structural defects as well as organization in the short range. Group theory calculations reported 24 Raman-active modes for orthorhombic C_{2v} symmetry of CT, with space group *Pbnm* and four clusters per unit cell ($Z^B = 4$) that are shown by irreducible representation (1) [31]. These modes are related to the stretching, torsional and bending vibrations of the metal–oxygen bonds in the CT crystal:

$$\Gamma_{(Raman)} = 7A_g + 5B_{1g} + 7B_{2g} + 5B_{3g} \quad (1)$$

Nevertheless, most of the modes cannot be detected because of their low polarizabilities caused by the HTMW methodology. This methodology is responsible by the interaction between the ions which promote the overlapping of some Raman active modes with others modes of low intensity [32,33]. As a result, only nine Raman-active modes are observed to orthorhombic $CaTiO_3$ perovskite-type crystalline structure, represented as P_1, P_2, P_3, P_4, P_5, P_6, P_7, P_8 and P_9 in Fig. 3.

The Raman mode P_1 corresponds to the orthorhombic structure of the CT. The modes P_2, P_3, P_4, P_5 and P_6 correspond to vibrational modes of the bond angles O–Ti–O.

The modes P_7 and P_8 correspond to a torsional mode in the Ti–O_6 bonds and the peak at P_9 correspond to the symmetric stretching mode of Ti–O bonds [33]. Table 1 list the peaks assigned to the CT, CT0.5, CT1, CT3 and CT5 microcrystals. The values were compared with those related in the literature.

As can be observed in this table, peak positions presented in this work are close to the reported by the literature and no deviations were observed, which confirm that Sm^{3+} content did not cause distortions and defects into lattice at shot range. It was also verified that micro-Raman vibrational modes are present for all the samarium concentration employed, indicating the orthorhombic phase of the material which is in agreement with the XRD patterns.

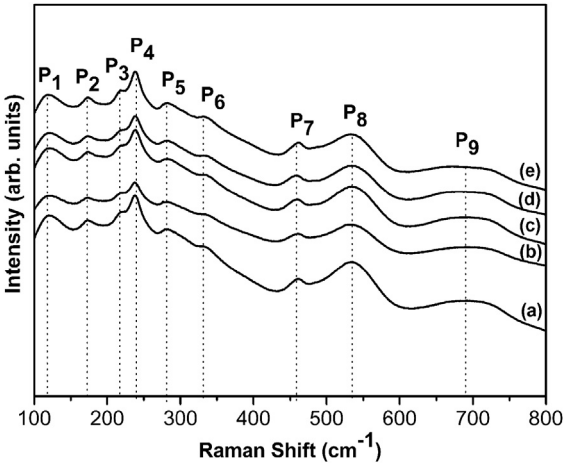

Fig. 3. Micro-Raman Scattering spectra of (a) CT, (b) CT0.5, (c) CT1, (d) CT3 and (e) CT5 powders synthesized at 140 °C for 16 min.

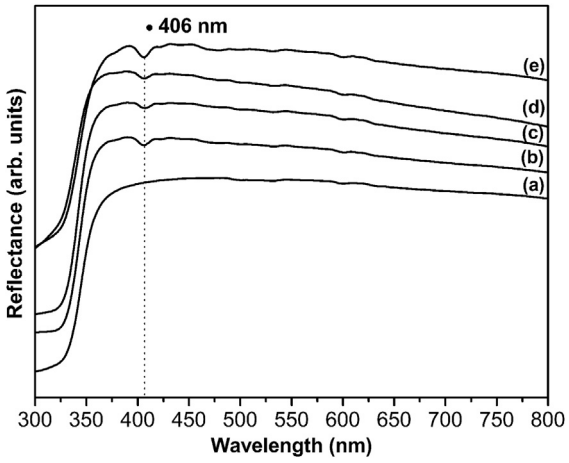

Fig. 4. Diffused reflectance spectra of (a) CT, (b) CT0.5, (c) CT1, (d) CT3 and (e) CT5 powders synthesized at 140 °C for 16 min.

Table 1
Data of micro-Raman scaterring spectra observed for CT, CT0.5, CT1, CT3 and CT5 powders synthesized at 140 °C for 16 min compared with those related in the literature.

Modes		Wavenumber (cm^{-1})		
	Fig. 3	Reference [37]	Reference [56]	This work
Ca–TiO_3 lattice mode	P_1	134	155	120
O–Ti–O bending mode	P_2	181	180	172
	P_3	224	226	219
	P_4	244	247	237
	P_5	287	286	280
	P_6	339	337	333
Ti–O_3 torsional mode	P_7	464	471	457
	P_8	537	495	534
Ti–O stretching mode	P_9	669	639	688

3.3. Ultraviolet visible spectroscopy (UV–vis)

Nearly ordered structure was verified through diffuse reflectance spectra being this technique indicated for the study of optical behavior of the samples. Fig. 4 shows the diffused reflectance spectra of the samples synthesized at 140 °C for 16 min. The presence of a peak at 406 nm corresponding to $^6H_{5/2} \rightarrow {}^4F_{7/2}$ transition for all doped powders indicates the Sm^{3+} ion in the lattice. This peak is also observed in excitation spectra of CT:Sm samples.

The impurity as result of doping may impact the electronic structure of the host, namely the band gap energy, so it was calculated by the Kubelka and Munk-Aussig [34]. This methodology is based on the transformation of diffuse reflectance measurements to estimate E_{gap} values with good accuracy within the limits of assumptions when modeled in three dimensions [35]. It is particularly useful in limited cases of an infinitely thick sample layer. The Kubelka–Munk equation for any wavelength is described as

$$F(R_\infty) = \frac{(1-R_\infty)^2 k}{2R_\infty s} \quad (2)$$

where $F(R_\infty)$ is the Kubelka–Munk function or absolute reflectance of the sample. In our case, magnesium oxide (MgO) was the standard sample in reflectance measurements. $R_\infty = R_{sample}/R_{MgO}$ (R is the reflectance when the sample is infinitely thick), k is the molar absorption coefficient and s is the scattering coefficient. In a parabolic band structure, the optical band gap and absorption coefficient of semiconductor oxides [36] can be calculated by the following equation:

$$\alpha h\nu = C_1(h\nu - E_{gap})^n \quad (3)$$

where α is the linear absorption coefficient of the material, $h\nu$ is the photon energy, C_1 is a proportionality constant, E_{gap} is the optical band gap and n is a constant associated with the different kinds of electronic transitions that for this material is $n = 1/2$ (direct allowed transitions) [37]. Finally, using the remission function described in Eq. (2) and with the term $k = 2\alpha$ and C_2 as a proportionality constant, we obtain the modified Kubelka–Munk equation:

$$[F(R_\infty)h\nu]^2 = C_2(h\nu - E_{gap}) \quad (4)$$

Therefore, finding the $F(R_\infty)$ value from Eq. (4) and plotting a graph of $[F(R_\infty)h\nu]^2$ against $h\nu$, the E_{gap} values of the samples were determined.

The band gap of CT and CT:Sm samples were calculated being the values 3.61, 3.44, 3.42, 3.33 and 3.41 eV for CT, CT0.5, CT1, CT3 and CT5 respectively. The maximum value correspond to the structure of higher symmetry, and once CT:Sm samples showed little decrease in the band gap, it can be concluded Sm^{3+} content created small defects in the material, due to creation of intermediary level in the band gap.

3.4. Photoluminescence (PL) Properties of CT:Sm samples

Optical properties such as PL depend on both structural and electronic properties, including compositional ordering and the presence of impurities and defects. PL spectroscopy is a fundamental technique to obtain information about the electronic structure as well as optical and photoelectronic properties of the materials including gap states and shallow and deep defects. PL depends on the electronic excitations and thus is a necessary complement to spectroscopy concerning lattice excitations, yielding structural information of a completely different character from the information obtainable by diffraction-based techniques since the latter detect long-range order while the former yield information on the intermediate surroundings of a luminescent cluster. Thus this technique is particularly useful as a structural probe in intermediate range disordered structures [38].

The excitation spectra of CT:Sm phosphors monitored at 648 nm which corresponds to hypersensitive $^4G_{5/2} \rightarrow {}^6H_{9/2}$ transition is presented in Fig. 5. The bands assigned in the spectra correspond from Sm^{3+} ground state $^6H_{5/2}$ to the higher energy states $^4D_{3/2}$, $^6P_{7/2}$, $^4M_{21/2}$, $^4F_{7/2}$, $^6P_{5/2}$, $^4G_{9/2}$, $^4I_{13/2}$, $^4I_{9/2}$ and $^4F_{3/2}$ at 365, 378, 391, 406, 421, 439, 463, 479 and 529 nm, respectively, and were attributed based on energetic levels positions [39]. Most of these bands have forced electric-dipole contribution ($\Delta J \leq 6$), and few have magnetic-dipole contribution ($\Delta J = 0, \pm 1$). All samples present the same patterns and the maximum intensity transition occurred in 406 nm ascribed to $^6H_{5/2} \rightarrow {}^4F_{7/2}$ transition, so this band was chosen as the excited light. It is shown only direct excitation of Sm^{3+} ions once Sm^{3+} interaction with the host lattice is weak and is unlikely to occur energy transfer between Sm^{3+} and the host.

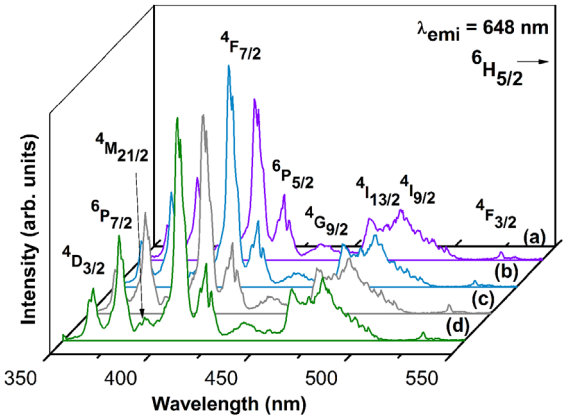

Fig. 5. Excitation spectra of (a) CT0.5, (b) CT1, (c) CT3 and (d) CT5 powders synthesized at 140 °C for 16 min, purchased by fixing the emission wavelength at 648 nm.

The emission spectra of CT:Sm phosphors with fixed excitation corresponding to $^6H_{5/2} \rightarrow {}^4F_{7/2}$ transition at 406 nm are shown in Fig. 6. The emission bands are from the intra 4f transitions of Sm^{3+}, and the principals for this material are $^4G_{5/2} \rightarrow {}^6H_{5/2}$, $^4G_{5/2} \rightarrow {}^6H_{7/2}$, $^4G_{5/2} \rightarrow {}^6H_{9/2}$ and $^4G_{5/2} \rightarrow {}^6H_{11/2}$ at 567, 603, 648 and 713 nm, respectively. Between these, $^4G_{5/2} \rightarrow {}^6H_{7/2}$ and $^4G_{5/2} \rightarrow {}^6H_{9/2}$ transitions have strongest intensities, which contribute to orange emission of the material. These transitions are useful specially in color displays [40,41].

In Fig. 6B is plotted the intensity of the strongest peak of the CT:Sm samples localized in 648 nm corresponding to $^4G_{5/2} \rightarrow {}^6H_{9/2}$ transition as a function of Sm^{3+} concentration. As Sm^{3+} doping concentration increased, enhancement of the photoluminescence intensity was observed up to 1 mol% and then decrease, but the shape and position of peaks did not change during this process. So, for 1 mol% concentration, quenching is observed. For 0.5% the lower doping concentration causes weak luminescence. The quenching appears because of nearest neighboring excited ions and the rise in the number of non-radiative decays which occurred due to energy transfer processes between excited and unexcited Sm^{3+} ions [9,42], caused by a decrease in the number of optically active Sm^{3+} ions [41]. Once all the spectra were taken at room temperature, it is not possible to affirm if quenching observed was because of thermal phonons [21].

Since Sm^{3+} is an odd-electron system, in all site symmetries except cubic and octahedral, the intraconfigurational

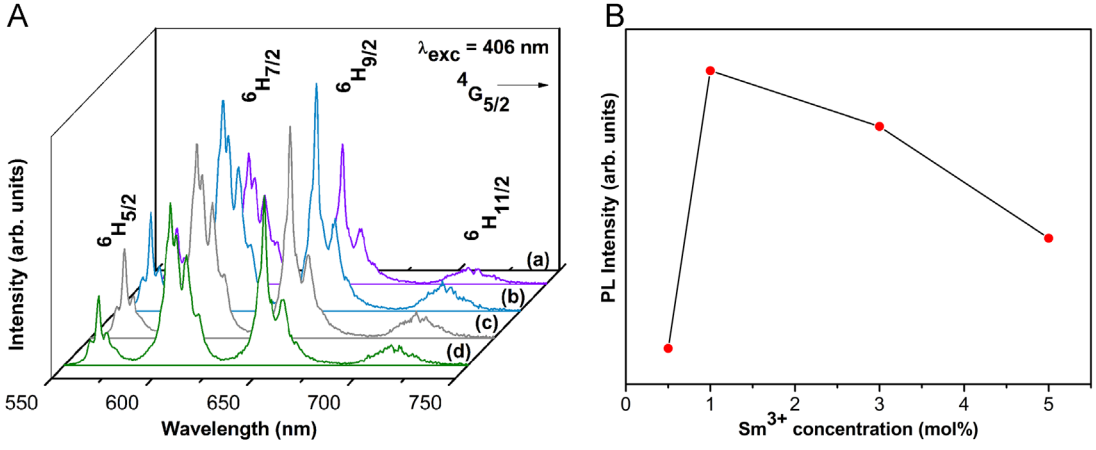

Fig. 6. (A) Emission spectra of (a) CT0.5, (b) CT1, (c) CT3 and (d) CT5 powders synthesized at 140 °C for 16 min, purchased by fixing the excitation wavelength at 406 nm. (B) PL Intensity of $^4G_{5/2} \rightarrow {}^6H_{9/2}$ transition as a function of Sm^{3+} concentration.

transitions in all samples split into the maximum number of $(J+½)$ manifolds, suggesting that Sm^{3+} ion occupies a local site with lower symmetry (C_{nv}, C_n or C_s) [43]. Since the energy gap between the $^4G_{5/2}$ emission level and the next lower lying $^6F_{11/2}$ level is nearly 7000 cm^{-1}, five phonons with the highest energy of 1350 cm^{-1} would be necessary to link this energy gap and the multiphonon non-radiative decay is impossible to occur. So, radiative transitions and energy transfer through cross-relaxations are the main responsible processes which de-populate the excited $^4G_{5/2}$ state [12,44]. Fig. 7 illustrate the energy level diagram of the four main PL transitions which occurred for our system using Sm^{3+}.

Magnetic dipole transitions obey the selection rule of $\Delta J=0$ and ± 1, and electric dipole transitions obey the selection rule of $\Delta J \leq 6$ unless J or $J'=0$ when $\Delta J=2$, 3, 6 [45]. The transitions $^4G_{5/2}\rightarrow{}^6H_{5/2}$ and $^4G_{5/2}\rightarrow{}^6H_{7/2}$ are magnetic dipole dominated, while the transitions $^4G_{5/2}\rightarrow{}^6H_{9/2}$ and $^4G_{5/2}\rightarrow{}^6H_{11/2}$ are electric dipole dominated [46]. The local symmetry of Sm^{3+} was measured with the relative intensity of the electric-dipole $^4G_{5/2}\rightarrow{}^6H_{9/2}$ transition and the magnetic-dipole $^4G_{5/2}\rightarrow{}^6H_{5/2}$ transition. As the former is sensitive to the environment and is more intense, it is known as hypersensitive while the latter is little affected by the environment. The ratio of these transitions were calculated for all CT:Sm powders being the values of the as-synthesized samples 3.09, 3.19, 3.25 and 3.32 for CT0.5, CT1, CT3 and CT5 respectively. These values shown little change as Sm^{3+} content increased up to 5%, which means these ions are in a symmetric state rather than in a distorted environment.

According to discussions in the literature there is an order–disorder concept [47] in materials such as glasses [48], amorphous materials [49], and ceramics [50] to explain some properties of these solid solutions. In a structurally disordered solid is no complete order of atoms positions. The aforementioned experimental results strongly indicate that photoluminescence is directly related to the structural disorder. A detailed understanding of so-called structural order–disorder and of the PL phenomenon from the structural point of view obviously requires a detailed knowledge of the atomic-scale structure.

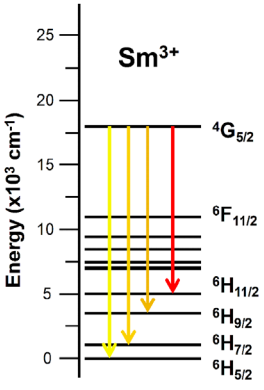

Fig. 7. Energy level diagram of the main PL transitions which occurred for our system using Sm^{3+}.

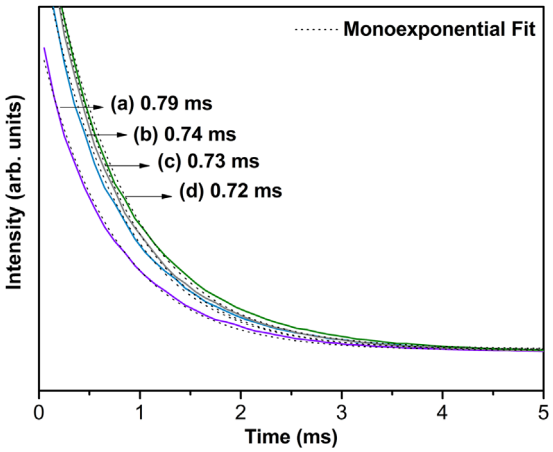

Fig. 8. Lifetime decay curves and monoexponential fit of the Sm^{3+} transition ($^4G_{5/2}\rightarrow{}^6H_{9/2}$) for the CT:Sm powders synthesized at 140 °C for 16 min. (a) CT0.5, (b) CT1, (c) CT3 and (d) CT5.

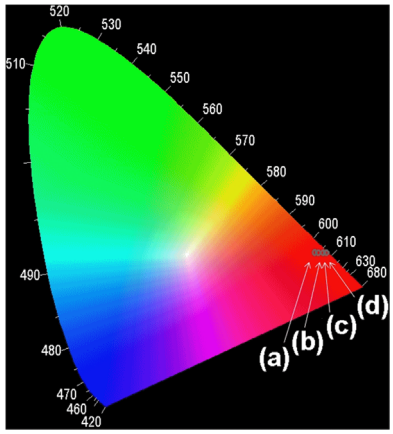

Fig. 9. The CIE chromaticity diagram for (a) CT0.5, (b) CT1, (c) CT3 and (d) CT5 powders synthesized at 140 °C for 16 min.

3.5. Lifetime

The lifetimes of the as-prepared samples were calculated on the basis of luminescence decay of $^4G_{5/2}\rightarrow{}^6H_{9/2}$ transition for the CT:Sm powders synthesized at 140 °C for 16 min, using emission and excitation of Sm^{3+} at 648 and 406 nm, respectively. Fig. 8 illustrate the monoexponential decay of all samples which were well fitted into a single exponential function [9] as shown is Eq. (5).

$$y = y_0 + A_1 \exp\left(\frac{-t}{\tau}\right) \quad (5)$$

where y_0 and y are intensities at zero time and at time t, respectively, A_1 is the signal amplitude and τ is the lifetime for transition selected. Plots of log(y) versus t for the samples were done and fitted into a linear fit indicating the samples have only one time of decay.

The values of decay time for the samples obtained through Eq. (5) are also depicted in Fig. 8. The decay time was evaluated as around 0.8 ms to Sm^{3+} concentration of $x=0.5$, and then begins to decrease smoothly as the Sm^{3+} content increases. This

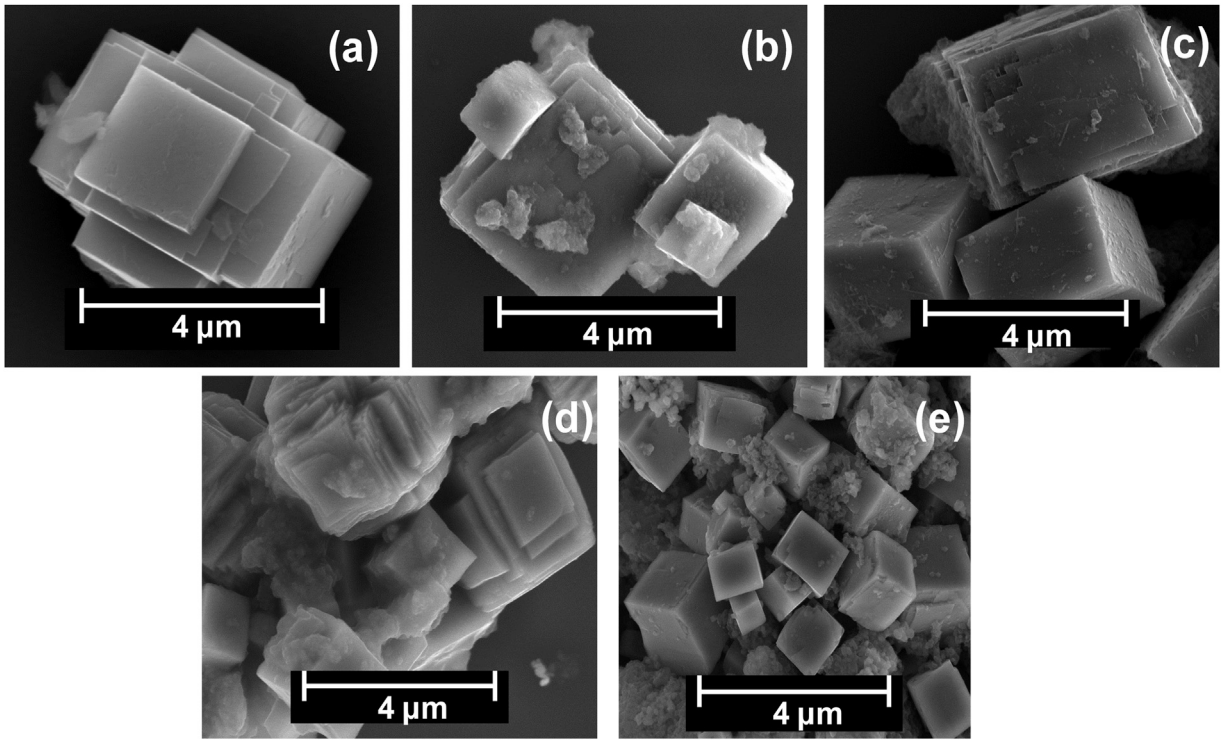

Fig. 10. FE-SEM micrograph of CT and CT:Sm powders synthesized at 140 °C for 16 min. (a) CT, (b) CT0.5, (c) CT1, (d) CT3 and (e) CT5.

behavior is in accordance with the quenching results, since the energy transfer occurred between Sm^{3+} ions in the lattice [51]. Moreover, Yu et al. [52] attributed this monoexponential decay when the distribution of Sm^{3+} in the matrix is homogeneous. According to these data, Sm^{3+} ions occupy only one site of symmetry in the CT matrix. This assumption is supports by the XRD and MRS results, which for our system showed that Sm^{3+} ions are located preferably in the A site of the CT framework.

3.6. CIE

The Commission International d'Eclairage (CIE) chromaticity coordinates is a tool to obtain information about brightness and efficiency of luminescence. The values for the samples are CT0.5 ($x=0.626$ $y=0.339$), CT1 ($x=0.636$ $y=0.338$), CT3 ($x=0.647$ $y=0.338$) and CT5 ($x=0.654$ $y=0.339$), being all values localized in the orange emission region (Fig. 9). Throughout these analyses it could predict the dominant wavelength occured around 648 nm, corresponding to $^4G_{5/2} \rightarrow {}^6H_{9/2}$ transition. These results are very closed to others Sm materials [53] and once the points are close to an specified color region, this indicates all the samples are appropriate to act as efficient visible phosphors.

3.7. FE-SEM

Fig. 10 shows FE-SEM images of CT and CT:Sm synthesized by the HTMW method. Fig. 10 (a), (b), (c), (d) and (e) stands for CT, CT0.5, CT1, CT3 and CT5, respectively. It is possible to see regular micro-cube morphology to all samples similar to calcite crystal that is formed through self-assemble of nanoplates [54]. The average sizes of the cubes are 3.0 μm, and the increase of Sm^{3+} concentration did not change the morphology, once the quantity utilized was small. This morphology and size can be explained in terms of the microwave irradiation exposure, which is not seen in others papers using different methodologies [55].

4. Conclusions

CT and CT:Sm perovskite-type materials were obtained using low temperature, short reactional time and low concentrations of the rare earth ions, being the first time CT:Sm samples prepared by this methodology. The spectroscopic photoluminescence of Samarium were useful to create new phospors in the orange range visible spectra. The profile of the lifetime decay curves reveals the presence of only one site of symmetry, which was occupied by Sm^{3+} ion in the CT matrix, which supports XRD and MRS analyses. The XRD and MRS confirmed the order of the as-prepared materials in long and short-range, respectively. The micro-cube shape of these materials was not changed by the Sm^{3+} concentrations utilized here. It can be concluded that all samples were obtained using an environmentally friendly process, potentially allowing the materials to be used in luminescent devices.

Acknowledgments

The authors appreciate the support of the Brazilian research financing institutions: grant#573636/2008-7 (CNPq), grant#2008/57872-1 (São Paulo Research Foundation, FAPESP), grant#2013/07296-2 (São Paulo Research Foundation, FAPESP-CDMF) and

grant#132320/2012-6 (CNPq). They also wish to thanks to Rorivaldo Camargo, Sergio (UNESP-Araraquara) and Madalena Tursi for technical and scientific contributions.

References

[1] S. Som, A.K. Kunti, V. Kumar, V. Kumar, S. Dutta, M. Chowdhury, S. K. Sharma, J.J. Terblans, H.C. Swart, Defect correlated fluorescent quenching and electron phonon coupling in the spectral transition of Eu^{3+} in $CaTiO_3$ for red emission in display application, J. Appl. Phys. 115 (2014) 193101.

[2] T.M. Mazzo, I.M. Pinatti, L.R. Macario, W. Avansi Junior, M.L. Moreira, I.L.V. Rosa, V.R. Mastelaro, J.A. Varela, E. Longo, Europium-doped calcium titanate: optical and structural evaluations, J. Alloy. Compd. 585 (2014) 154–162.

[3] L.S. Cavalcante, V.M. Longo, J.C. Sczancoski, M.A.P. Almeida, A. A. Batista, J.A. Varela, M.O. Orlandi, E. Longo, M.S. Li, Electronic structure, growth mechanism and photoluminescence of $CaWO_4$ crystals, CrystEngComm 14 (2012) 853.

[4] P.K. Mallik, B. Basu, Better early osteogenesis of electroconductive hydroxyapatite-calcium titanate composites in a rabbit animal model, J. Biomed. Mater. Res. A 102 (2014) 842–851.

[5] H. Zheng, G.D.C. Csete de Györgyfalva, R. Quimby, H. Bagshaw, R. Ubic, I.M. Reaney, J. Yarwood, Raman spectroscopy of B-site order–disorder in $CaTiO_3$-based microwave ceramics, J. Eur. Ceram. Soc. 23 (2003) 2653–2659.

[6] H. Mizoguchi, K. Ueda, M. Orita, S.-C. Moon, K. Kajihara, M. Hirano, H. Hosono, Decomposition of water by a $CaTiO_3$ photocatalyst under UV light irradiation, Mater. Res. Bull. 37 (2002) 2401–2406.

[7] S. Okamoto, H. Yamamoto, Characteristic enhancement of emission from $SrTiO_3:Pr^{3+}$ by addition of group-IIIb ions, Appl. Phys. Lett. 78 (2001) 655–657.

[8] T.M. Mazzo, M.L. Moreira, I.M. Pinatti, F.C. Picon, E.R. Leite, I.L. V. Rosa, J.A. Varela, L.A. Perazolli, E. Longo, $CaTiO_3:Eu^{3+}$ obtained by microwave assisted hydrothermal method: a photoluminescent approach, Opt. Mater. 32 (2010) 990–997.

[9] G. Blasse, B.C. Grabmaier, Luminescent Materials, 1st ed., Springer-Verlag, Berlin, 1994.

[10] C.A. Kodaira, R. Stefani, A.S. Maia, M.C.F.C. Felinto, H.F. Brito, Optical investigation of $Y_2O_3:Sm^{3+}$ nanophosphor prepared by combustion and Pechini methods, J. Lumin. 127 (2007) 616–622.

[11] M.S. Kim, L. Krishna Bharat, J.S. Yu, White light emission characteristics of Tb^{3+} and Sm^{3+} co-doped $CaYAlO_4$ nanocrystalline phosphors for solid-state lighting, J. Lumin. 142 (2013) 92–95.

[12] D. Umamaheswari, B.C. Jamalaiah, T. Sasikala, I.-G. Kim, L. R. Moorthy, Photoluminescence properties of Sm^{3+}-doped SFB glasses for efficient visible lasers, J. Non-Cryst. Solids 358 (2012) 782–787.

[13] V.V. Ursaki, V. Lair, L. Živković, M. Cassir, A. Ringuedé, O. Lupan, Optical properties of Sm-doped ceria nanostructured films grown by electrodeposition at low temperature, Opt. Mater. 34 (2012) 1897–1901.

[14] K.E. Knope, D.T. de Lill, C.E. Rowland, P.M. Cantos, A. de Bettencourt-Dias, C.L. Cahill, Uranyl sensitization of samarium(III) luminescence in a two-dimensional coordination polymer, Inorg. Chem. 51 (2012) 201–206.

[15] G.-H. Lee, T.-H. Kim, C. Yoon, S. Kang, Effect of local environment and Sm^{3+}-codoping on the luminescence properties in the Eu^{3+}-doped potassium tungstate phosphor for white LEDS, J. Lumin. 128 (2008) 1922–1926.

[16] M. Mitric, J. Blanusa, T. Barudzija, Z. Jaglicic, V. Kusigerski, V. Spasojevic, Magnetic properties of trivalent Sm ions in $Sm_xY_{2-x}O_3$, J. Alloy. Compd. 485 (2009) 473–477.

[17] S.B. Stevens, C. Morrison, Emission measurements and crystal-field calculations for $^4G_{5/2}$ to $^6H_{7/2}$ transitions in Sm^{3+}:YAG, J. Appl. Phys. 70 (1991) 948–953.

[18] B. Tyliszczak, K.Z. Gaca, A. Sobczak-Kupiec, P. Dulian, Mechano-chemical synthesis and investigations of calcium titanate powders and their acrylic dispersions, J. Eur. Ceram. Soc. 34 (2014) 2259–2264.

[19] T.R.N. Kutty, R. Vivekanandan, P. Murugaraj, Precipitation of rutile and anatase (TiO_2) fine powders and their conversion to $BaTiO_3$, $SrTiO_3$, $CaTiO_3$ by hydrothermal method, Mater. Chem. Phys. 19 (1988) 533–546.

[20] X. Zhang, H. Zhang, X. Ren, X.-J. Wang, The dependence of persistent phosphorescence on annealing temperatures in $CaTiO_3:Pr^{3+}$ nanoparticles prepared by a coprecipitation technique, J. Solid State Chem. 181 (2008) 393–398.

[21] M.G. Ha, M.R. Byeon, T.E. Hong, J.S. Bae, Y. Kim, S. Park, H.-S. Yang, K.S. Hong, Sm^{3+}-doped $CaTiO_3$ phosphor: synthesis, structure, and photoluminescent properties, Ceram. Int. 38 (2012) 1365–1370.

[22] A.T. de Figueiredo, S. de Lazaro, E. Longo, E.C. Paris, J.A. Varela, M. R. Joya, P.S. Pizani, Correlation among order–disorder, electronic levels, and photoluminescence in amorphous CT:Sm, Chem. Mater. 18 (2006) 2904–2911.

[23] A.T. de Figueiredo, V.M. Longo, R.O. da Silva, V.R. Mastelaro, A. Mesquita, R.W.A. Franco, J.A. Varela, E. Longo, Structural XANES characterization of $Ca_{0.99}Sm_{0.01}TiO_3$ perovskite and correlation with photoluminescence emission, Chem. Phys. Lett. 544 (2012) 43–48.

[24] A.T. de Figueiredo, V.M. Longo, S. de Lazaro, V.R. Mastelaro, F.S. De Vicente, A.C. Hernandes, M. Siu, Li, J.A. Varela, E. Longo, Blue-green and red photoluminescence in $CaTiO_3$:Sm, J. Lumin. 126 (2007) 403–407.

[25] E.C. Paris, M.F.C. Gurgel, M.R. Joya, G.P. Casali, C.O. Paiva-Santos, T. M. Boschi, P.S. Pizani, J.A. Varela, E. Longo, Structural deformation monitored by vibrational properties and orbital modeling in $(Pb,Sm)TiO_3$ systems, J. Phys. Chem. Solids 71 (2010) 12–17.

[26] X. Zhang, J. Zhang, X. Zhang, L. Chen, Y. Luo, X.-j Wang, Enhancement of the red emission in $CaTiO_3:Pr^{3+}$ by addition of rare earth oxides, Chem. Phys. Lett. 434 (2007) 237–240.

[27] K. Ohnuma, N. Ozaki, Y. Mizuno, T. Hagiwara, K.I. Kakimoto, H. Ohsato, Occupational sites of Sm in $BaTiO_3$ analyzed by rietveld method and EXAFS, Ferroelectrics 332 (2006) 7–11.

[28] S. Okamoto, H. Yamamoto, Emission from $BaTiO_3:Pr^{3+}$ controlled by ionic radius of added trivalent ion, J. Appl. Phys. 91 (2002) 5492.

[29] D. Makovec, Z. Samardzija, D. Kolar, Solid solubility of cerium in $BaTiO_3$, J. Solid State Chem. 123 (1996) 30–38.

[30] K. Momma, F. Izumi, VESTA 3 for three-dimensional visualization of crystal, volumetric and morphology data, J. Appl. Crystallogr. 44 (2011) 1272–1276.

[31] S. Qin, X. Wu, F. Seifert, A.I. Becerro, Micro-Raman study of perovskites in the $CaTiO_3$–$SrTiO_3$ system, J. Chem. Soc., Dalton Trans. (2002) 3751–3755.

[32] T. Hirata, K. Ishioka, M. Kitajima, Vibrational spectroscopy and X-ray diffraction of perovskite compounds $Sr_{1-x}M_xTiO_3$ (M=Ca, Mg; $0 < x < 1$), J. Solid State Chem. 124 (1996) 353–359.

[33] H. Zheng, I.M. Reaney, G.D.C.C. de Györgyfalva, R. Ubic, J. Yarwood, M.P. Seabra, V.M. Ferreira, Raman spectroscopy of $CaTiO_3$-based perovskite solid solutions, J. Mater. Res. 19 (2004) 488–495.

[34] P. Kubelka, F. Munk, An article on optics of paint layers, Zeit. Für. Tech. Phys. 12 (1931) 593.

[35] M.L. Myrick, M.N. Simcock, M. Baranowski, H. Brooke, S.L. Morgan, J. N. McCutcheon, The Kubelka–Munk diffuse reflectance formula revisited, Appl. Spectrosc. Rev. 46 (2011) 140–165.

[36] D. Wood, J. Tauc, Weak absorption tails in amorphous semiconductors, Phys. Rev. B 5 (1972) 3144–3151.

[37] M.L. Moreira, E.C. Paris, G.S. do Nascimento, V.M. Longo, J. R. Sambrano, V.R. Mastelaro, M.I.B. Bernardi, J. Andrés, J.A. Varela, E. Longo, Structural and optical properties of $CaTiO_3$ perovskite-based materials obtained by microwave-assisted hydrothermal synthesis: an experimental and theoretical insight, Acta Mater. 57 (2009) 5174–5185.

[38] V.M. Longo, M. das Graca Sampaio Costa, A. Zirpole Simoes, I.L. Rosa, C.O. Santos, J. Andres, E. Longo, J.A. Varela, On the photoluminescence behavior of samarium-doped strontium titanate nanostructures under UV light. A structural and electronic understanding, Phys. Chem. Chem. Phys. 12 (2010) 7566–7579.

[39] W.T. Carnall, G.L. Goodman, K. Rajnak, R.S. Rana, A systematic analysis of the spectra of the lanthanides doped into single crystal LaF_3, J. Chem. Phys. 90 (1989) 3443.

[40] S. Sailaja, S.J. Dhoble, B. Sudhakar Reddy, Synthesis and photoluminescence properties of Sm^{3+} and Dy^{3+} ions activated $Ca_2Gd_2W_3O_{14}$ phosphors, J. Mol. Struct. 1003 (2011) 115–120.

[41] İ. Pekgözlü, S. Çakar, Photoluminescence properties of $Li_6CaB_3O_{8.5}$: M^{3+} (M^{3+}: Dy and Sm), J. Lumin. 132 (2012) 2312–2317.

[42] Y.-C. Li, Y.-H. Chang, Y.-F. Lin, Y.-S. Chang, Y.-J. Lin, Synthesis and luminescent properties of Ln^{3+} (Eu^{3+}, Sm^{3+}, Dy^{3+})-doped lanthanum aluminum germanate $LaAlGe_2O_7$ phosphors, J. Alloy. Compd. 439 (2007) 367–375.

[43] C.A. Kodaira, H.F. Brito, E.E.S. Teotonio, M.C.F.C. Felinto, O.L. Malta, G.E.S. Brito, Photoluminescence behavior of the Sm^{3+} and Tb^{3+} ions doped into the $Gd_2(WO_4)_3$ matrix prepared by the Pechini and ceramic methods, J. Braz. Chem. Soc. 15 (2004) 890–896.

[44] C. Srinivasa Rao, C.K. Jayasankar, Spectroscopic and radiative properties of Sm^{3+}-doped K–Mg–Al phosphate glasses, Optic. Commun. 286 (2013) 204–210.

[45] Z. Cui, R. Ye, D. Deng, Y. Hua, S. Zhao, G. Jia, C. Li, S. Xu, Eu^{2+}/Sm^{3+} ions co-doped white light luminescence $SrSiO_3$ glass-ceramics phosphor for White LED, J. Alloy. Compd. 509 (2011) 3553–3558.

[46] J.F. Martel, S. Jandl, B. Viana, D. Vivien, Crystal field study of Sm^{3+} ions in Sm_2O_3, Sm^{3+}:Gd_2O_3 and Sm^{3+}:Y_2O_3, J. Phys. Chem. Solids 61 (2000) 1455–1463.

[47] G. Blasse, A. Bril, Photoluminescent efficiency of phosphors with electronic transitions in localized centers, J. Electrochem. Soc. 115 (1968) 1067–1075.

[48] F. Sciortino, Disordered materials: one liquid, two glasses, Nat. Mater. 1 (2002) 145–146.

[49] T.C. Hufnagel, Finding order in disorder, Nat. Mater. 3 (2004) 666–667.

[50] C. Malibert, B. Dkhil, J.M. Kiat, D. Durand, J.F. Bérar, A.S.-d Biré, Order and disorder in the relaxor ferroelectric perovskite $PbS_{c1/2}Nb_{1/2}O_3$ (PSN): comparison with with simple perovskites $BaTiO_3$ and $PbTiO_3$, J. Phys.: Condens. Matter 9 (1997) 7485–7500.

[51] J.S. Kumar, K. Pavani, T. Sasikala, A. Sreenivasa Rao, N.K. Giri, S.B. Rai, L. Rama Moorthy, Photoluminescence and energy transfer properties of Sm^{3+} doped CFB glasses, Solid State Sci. 13 (2011) 1548–1553.

[52] M. Yu, J. Lin, Z. Wang, J. Fu, S. Wang, H.J. Zhang, Y.C. Han, Fabrication, patterning, and optical properties of nanocrystalline YVO_4:A (A=Eu^{3+}, Dy^{3+}, Sm^{3+}, Er^{3+}) phosphor films via sol–gel soft lithography, Chem. Mater. 14 (2002) 2224–2231.

[53] X. Liu, J. Lin, Synthesis and luminescent properties of $LaInO_3$:RE^{3+} (RE=Sm, Pr and Tb) nanocrystalline phosphors for field emission displays, Solid State Sci. 11 (2009) 2030–2036.

[54] S. Saïd, P. Marchet, T. Merle-Méjean, J.-P. Mercurio, Raman spectroscopy study of the $Na_{0.5}Bi_{0.5}TiO_3$–$PbTiO_3$ system, Mater. Lett. 58 (2004) 1405–1409.

[55] T.M. Mazzo, L. Mendonça da Rocha Oliveira, L.R. Macario, W. Avansi, Rd Silveira André, I.L. Viana Rosa, J.A. Varela, E. Longo, Photoluminescence properties of $CaTiO_3$:Eu^{3+} nanophosphor obtained by the polymeric precursor method, Mater. Chem. Phys. 145 (2014) 141–150.

[56] U. Balachandran, N.G. Eror, Laser-induced Raman scattering in calcium titanate, Solid State Commun. 44 (1982) 815–818.